Progress In Electromagnetics Research M, Vol. 56, 53–61, 2017

A Novel Non-Coherent Micro-Doppler Imaging Method Using Hybrid Optimization

Mahdi Safari and Ali Abdolali*

Abstract—Conventional radar imaging methods use coherent analysis which highlights the necessity of signal phase measurement setups and complex inverse algorithms. To mitigate these drawbacks, this paper proposes a novel phase-less imaging algorithm. A nonlinear over-determined system of equations based on signal Doppler shift is developed, and a new error function originated from least square method is introduced. To obtain the exact position of targets, hybrid optimization is applied to the achieved error function. Simulation results demonstrate that the proposed method is well capable of detecting the targets containing strong point scatterers, even with the distance of 1 cm. Also, the resolution of imaging algorithm for point scatterer circumstances is obtained in the order of millimeter. Concurrent with the priory imaging algorithms with the same imaging setups using proposed method reduces complexity and increases imaging swiftness.

1. INTRODUCTION

Doppler shift phenomenon is used as a foundation for different imaging methods. It is mostly used to determine the speed of moving targets such as wind speed [1]. However, it is the basis of SAR (synthetic aperture radar) and ISAR (inverse synthetic aperture radar) imaging using phase variation obtained from coherent devices [2]. With the advent of imaging, there has been a focus in the literature on the advantages of this method and its supplementary method to make imaging methods capable of imaging moving targets. Also, there is a group of studies on different geometries of radar movement in the literature, which present imaging with circular SAR and ISAR [3, 4]. In this paper, a novel algorithm is proposed which can work along with the existing methods to improve imaging processes. Moreover, there are different complicated methods for solving inverse problems, namely inverse scattering [18–21], MUSIC [5], time reversal [19, 22], etc. The main disadvantages of the mentioned imaging methods are complexity, cost, and computational time; however, they are capable of reconstructing high-resolution. Since the inverse scattering methods reconstruct high-resolution images, they are suitable for medical imaging [19]. In this paper, novel method using non-coherent analysis is proposed which is capable of fast reconstruction of accurate images using new error function. One of the studies on imaging thin PECs using MUSIC algorithms was presented in [5]. In this paper, we present a new method for imaging stationary objects using Doppler phenomenon which uses time-dependent Doppler shift and phase less analysis. The proposed method uses moving transmitter and receiver and the relative speed between the object and radar in different positions to find the objects location. One of the advantages of the current method over others is its simplicity and computational time. Even without applying optimization to the mentioned method, the proposed error function is capable of constructing realtime images, as presented in the results. Also, the method can be used as an additional method along with other methods to gain higher resolution and reduce calculation time with the same setups. One well-cited assertion in the literature is the effect of moving target on imaging and abolishing image

Received 22 February 2017, Accepted 9 April 2017, Scheduled 19 April 2017
* Corresponding author: Ali Abdolali (abdolal@iust.ac.ir).
The authors are with the Department of Electrical Engineering, Iran University of Science and Technology, Narmak, Tehran, Iran.

blurring due to target maneuvering by time-frequency analysis [6–11]. However, little attention has been paid to the advantages of using moving radars and micro-Doppler for the imaging or location of static objects. The issues of using Doppler phenomenon for imaging in ultrasound and its resolution improvement have been addressed by several authors [12]. However, the current method can work aside with these methods in ultrasound domain to gain more accuracy than operating in the microwave which is suitable for under-water sonar systems. The reason of achieving higher accuracy in the ultrasound wave is the difference between sound and light speeds. Since lower speed causes higher frequency shift in this method, the accuracy of imaging in ultrasound domain is higher which we will discuss later in this study. Nevertheless, an unresolved issue is imaging by non-coherent devices and analysis based on the known radar movement path. Some disadvantages of the former methods have been the costs of receiving, analyzer devices, resolution of phase estimation, and estimation error of Doppler frequency shift. Also, it is worth mentioning that the current method is capable of detecting the angular position of scatterers without any optimization by locating the points with zero Doppler shift. The purpose of the current study is to present a new and simple method with less time and financial costs using Doppler shift for imaging the stationary objects containing scattering points in general based on the known radar movement path. We choose circular radar movement and 2-dimensional (2D) imaging for representation and validation; however, other geometries, namely multipath geometries, would be more accurate.

2. METHOD

The current method relies on the relative speed between radar and the object in different positions. In this section, we choose the geometry to validate the method. However, the current method is applicable to different geometries based on the movement of radar, namely linear, circular, etc. Symmetry and simplicity are the reasons for the chosen geometry; other geometries probably would give us more precise results. Fig. 1 illustrates the circular geometry of radar movement. The origin of Cartesian coordinates is located on the center of radar orbit. Scattering wave equation from point scatterer with distance

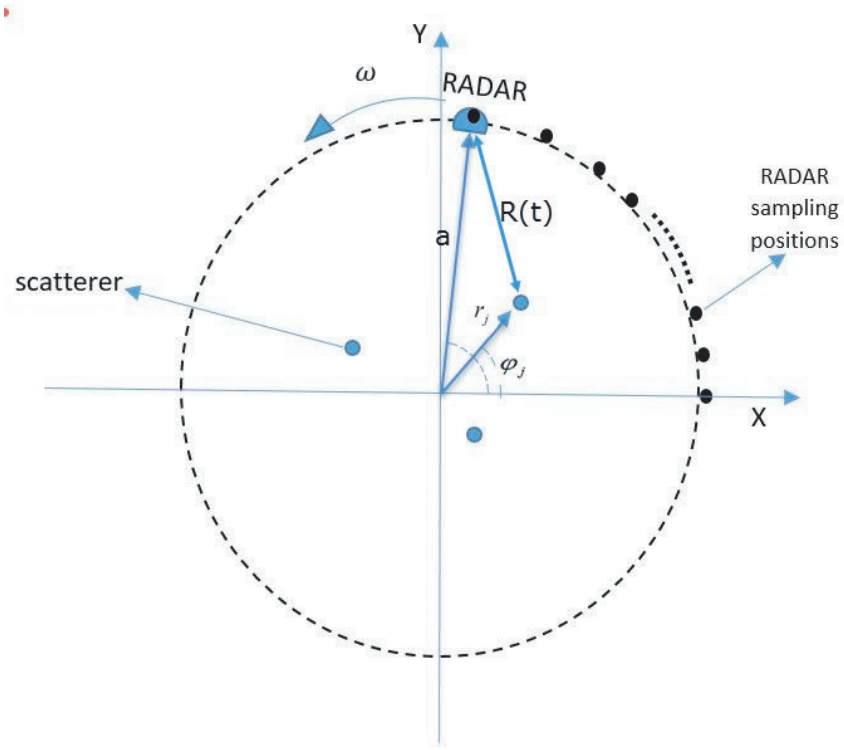

Figure 1. Imaging geometry.

vector $R(t)$ related to point source radar is as follows [13]:

$$s(t) = \rho \frac{e^{-i\mathbf{k}.\mathbf{R}(t)}}{|\mathbf{R}(t)|} \tag{1}$$

Since the rotational movement of radar is time-dependent and can be presented as $|\mathbf{R}(t)| = \left({r_j}^2 + a^2 - 2r_j a\cos(\omega t - \varphi_j)\right)^{1/2}$, and also the phase of the signal is:

$$\theta = -\frac{2\pi f}{c} 2\mathbf{R}(t), \tag{2}$$

the Doppler shift due to the radar movement in circular geometry with the presence of scatterers in the radar orbit plane is:

$$\Delta f_i = \frac{1}{2\pi}\frac{d\theta}{dt} = \frac{2a\omega f}{c} \frac{r_j \sin(\omega t_i - \varphi_j)}{\sqrt{({r_j}^2 + a^2 - 2r_j a\cos(\omega t_i - \varphi_j)}} \tag{3}$$

Here, Δf_i is the frequency shift in the ith sampling position, a the radius of radar orbit, C the speed of light in medium, f carrier frequency, ω the angular speed of radar, t_i the time at which we sample frequency shift, and (r, φ) the scatterer position in cylindrical coordinates. It is clear from Equation (3) that when radar and scatterer are in the same angular position, the resulting Doppler shift would be zero. The mentioned fact can help us to find the exact angular positions of the scatterers, by locating the radar sampling positions with zero frequency shift. If we sample frequency shift in N different positions, we will have N equations with 2 unknowns, which is an over-determined system of equation. A common solution for over-determined systems is the least square method which is used to find the values which minimize error [14]. Sum of squared error for the frequency shift system of the resulting equation is as follows:

$$\sum_{i=0}^{n} \left(\Delta f_i - \frac{2a\omega f}{c} \frac{r_j \sin(\omega t_i - \varphi_j)}{\sqrt{({r_j}^2 + a^2 - 2r_j a\cos(\omega t_i - \varphi_j)}} \right)^2 \tag{4}$$

in which n is the number of sampling positions. To find (r, φ) values which minimize the error, we use GA (genetic algorithms) [15]. Also, it is worth noting that the aforementioned error function is just suitable for single point scatterer scenario. It is clear from the equations that in the multi-point object, each point results in separate (different) time-dependent frequency shift signals, and we use optimization on these signals separately to find each point. To validate the imaging method, we use computer simulation using wave equation and STFT (short time frequency transform) to gain time-dependent frequency shift in the radar receiver due to several strong scattering points [16]. In this formula, ρ_{ij} is the reflectivity function of point scatterer, k the wave number, and $R(t)$ the displacement vector between radar and point scatterer. As mentioned earlier and considering the effect of multi-point scatterer, the return signal becomes:

$$s(t) = \sum_{m=1}^{N_r} \sum_{n=1}^{N_\varphi} \frac{\rho_{mn}\ e^{\frac{i2\pi f}{c} 2\left({r_m}^2 + a^2 - 2r_m a\cos(\omega t - \varphi_n)\right)^{1/2}}}{2({r_m}^2 + a^2 - 2r_m a\cos(\omega t - \varphi_n))^{1/2}} \tag{5}$$

To gain the time-varying spectrum of the receiving signal, we should use time-frequency transform. STFT is one of the simplest time-frequency transforms defined as [9]:

$$STFT(t, \omega) = \int_{-\infty}^{+\infty} s(\tau)\, w(\tau - t)\, e^{-i\Omega\tau} d\tau \tag{6}$$

Here, $w(\tau - t)$ is the window of STFT transform; in other words, it is the width of time samples for STFT. To gain information about the reflectivity function of point scatterer and strength of scatterer, we use the square modulus of STFT which is called spectrogram and defined as follows [17]:

$$spectrogram(t, \omega) = |STFT(t, \omega)|^2 \tag{7}$$

So, the spectrogram of the returned baseband signal becomes:

$$spectrogram(t, \omega) = \int_{-\infty}^{+\infty} \sum_{m=1}^{N_r} \sum_{n=1}^{N_\varphi} \rho_{mn} \frac{e^{\frac{i2\pi f}{c} 2({r_m}^2 + a^2 - 2r_m a\cos(\omega\tau - \varphi_n))^{\frac{1}{2}}}}{2({r_m}^2 + a^2 - 2r_m a\cos(\omega t - \varphi_n))^{\frac{1}{2}}} w(\tau - t) e^{-i\Omega\tau} \tag{8}$$

We can also replace sigma and integral:

$$spectrogram(t,\omega) = \sum_{m=1}^{N_r}\sum_{n=1}^{N_\varphi}\int_{-\infty}^{+\infty} \rho_{mn}\frac{e^{\frac{i2\pi f}{c}2({r_m}^2+a^2-2r_m a\cos(\omega\tau-\varphi_n))^{\frac{1}{2}}}}{2({r_m}^2+a^2-2r_m a\cos(\omega t-\varphi_n))^{\frac{1}{2}}}w(\tau-t)e^{-i\Omega\tau} \quad (9)$$

In this formula, ρ_{mn} is the element of $N_r \times N_\varphi$ reflectivity matrix ρ, and our aim is to image this matrix.

3. RESULTS

To attain the position of the objects, we use the time-varying spectrum obtained from STFT of receiving signal, replace time and frequency at the sampling points in the Doppler frequency shift error function, and use GA to find the (r, φ) values which minimize the error function of least square method. The imaging occurs in 2 different circumstances: point scatterer and multi-point scatterer.

3.1. Point Scatterer

This circumstance takes place when the radar is far enough from the object, which makes point scatterer's assumption feasible. In other words, the time-varying spectrum of receiving signal contains only one non-negligible component. To validate the imaging method in the point scatterer context, we set the previously-mentioned geometry properties by setting the radars orbiting around the circle with the radius of 2 m and angular speed of 12.57 rad/sec and point scatterer located in $(x, y) = (20\,\text{cm}, 20\,\text{cm})$ or $(r, \varphi) = (28.28\,\text{cm}, 0.7854\,\text{rad})$ position with the carrier frequency of 6 GHz. Fig. 2(a) demonstrates the spectrogram of the receiving signal due to the referred setup. We use maximum power spectrum to gain least square method's residual function and find (r, φ) which minimizes it. Fig. 2(b) demonstrates the logarithm of inverse residual function which is a suitable demonstration for scatterer's position and imaging.

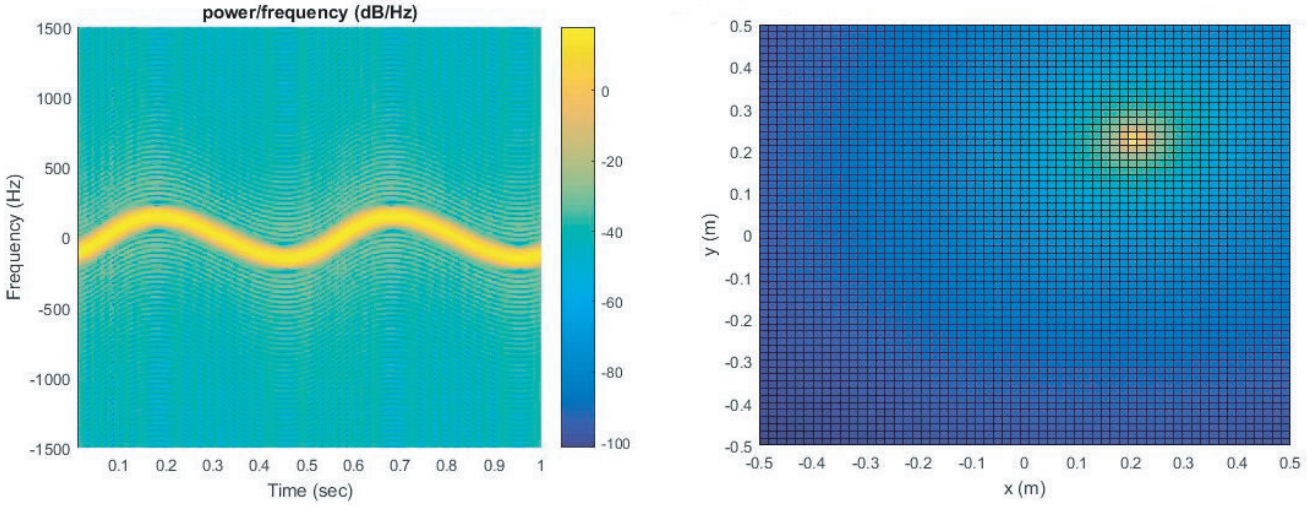

Figure 2. Point scatterer imaging. (a) Returned signal spectrum. (b) Inverse square error function.

As illustrated in Fig. 2(a), Doppler shift frequency is in 0–200 Hz range which is in the micro-Doppler range. Also, it is worth mentioning that according to the speed of sound in media such as water, ultrasound Doppler shift range will be increased and make this method more accurate. Due to least square method, (r, φ) which minimizes residual function is obtained as follows.

According to Table 1, imaging error is in mm which is one of the advantages of this method along with its simplicity. Also, it is worth noting that according to Doppler frequency shift's nonlinear equation, error is nonlinear and depends on the target position.

Table 1. Point scatterer and image position.

Point scatterers' position	Image position
$(x, y) = (0.20\,\text{m}, 0.20\,\text{m})$	$(x, y) = (0.199\,\text{m}, 0.199\,\text{m})$

3.2. Multi-Point Scatterer

Multi-point scatterers refer to the scatterers which have several points with high scattering, such as sharp edges. In other words, when the spectrum of a receiving signal contains more than one significant component, it can be reckoned as a multi-point scatterer. The recent method is applicable to the objects with strong point scatterers, such as a group of thin PECs or imaging of dielectrics with high contrasts. To achieve the positions of scatterers in the multi-point scenario, we introduce a new residual function based on least square method and point scatterer residual function. Multi-point residual function is represented as follows:

$$image(r, \theta) = \sum_{f} \sum_{t} \log\left(\frac{1}{error^2}\right) \tag{10}$$

$$error = \Delta f_i - \frac{2a\omega f}{C} \frac{r \sin(\omega t_i - \varphi)}{\sqrt{(r^2 + a^2 - 2ra\cos(\omega t_i - \varphi)}} \tag{11}$$

In the aforementioned function, the summation is operated on the frequency and time of the receiving signal spectrum. Figs. 3(c), (d) illustrate that the returned signal spectrum contains 4 components due to the imaging of 4-point scatterer at each sampling time. As (r, φ) approaches one of the scatterers' positions, the aforementioned error function approaches zero. Hence, local maximum is caused in the defined residual function which is illustrated in Fig. 3(b) for the 4-point scatterer scenario. To show the effect of the multi-point scatterer, we demonstrate the imaging of the random multi-point object in Fig. 4. The returned signal spectrogram is illustrated in Fig. 4(c), which shows different Doppler shifts due to different scatterer positions. To find the exact positions of the scatterers, we optimize the residual function using GA after deriving the angular positions of scatterers locating the radar sampling points with zero Doppler shift. Table 2 demonstrates the positions of the point scatterers and image. Also, it is worth noting that when the radar and scatterer have the same angle, Doppler shift becomes zero which means that the objects angle can be obtained from zero Doppler shifts in the returned signal spectrum components.

Table 2. Multi-point scatterers object and image positions.

Scatterer $(x(m), y(m))$	Image position
$(0.4, 0.06)$	$(0.3983, 0.0596)$
$(0.2, -0.2)$	$(0.1949, -0.1947)$
$(0, 0.4)$	$(0.0081, 0.4153)$
$(-0.36, 0.38)$	$(-0.3814, 0.4023)$
$(-0.2, 0.2)$	$(-0.2119, 0.2109)$
$(0.2, 0)$	$(0.2119, 0.0102)$
$(0.12, 0.06)$	$(0.1271, 0.0642)$
$(-0.2, -0.2)$	$(-0.2119, -0.2112)$

As presented in Table 2, the presented method is capable of multi-point imaging. Imaging errors are negligible compared with the radars orbit radius. It is also clear that the angular positions of the scatterers are derived rather exactly. At the end, it is worth mentioning that the residual function is the only criterion for presenting the position of objects; however, more accurate results are obtained

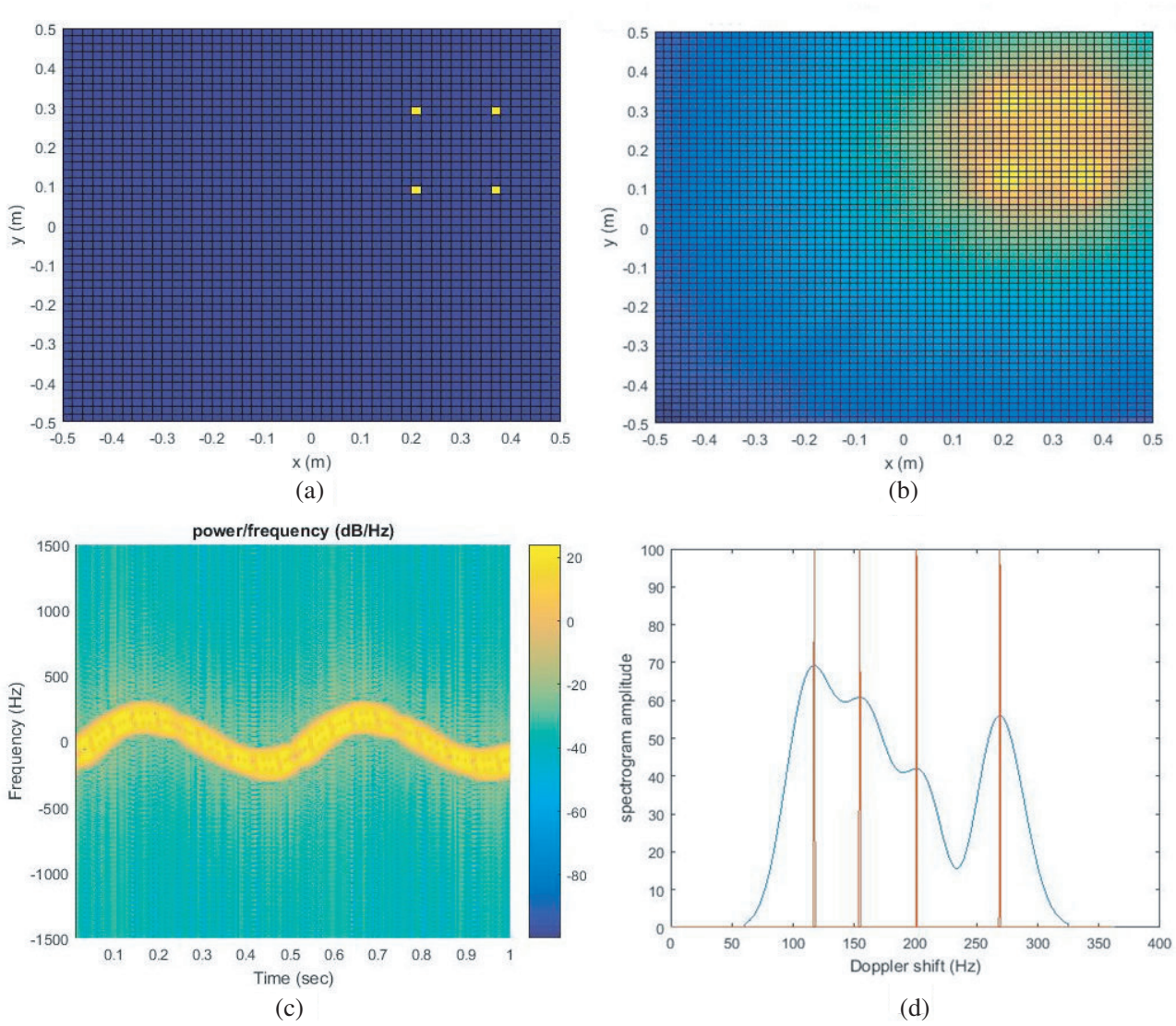

Figure 3. Imaging of a square (4 thin PEC). (a) Square scatterer. (b) Image. (c) Spectrum of the returned signal. (d) 4 components of Doppler shift at $t = 0.2\,\mathrm{s}$.

from optimization and illustrated in Table 2. It is also the reason for the opacity of Fig. 3(b) in the region of 2 near objects; however, Table 2 presents the separation of objects using the recent method. Table 3 illustrates the computational efficiency of the method.

The reason behind the less computation time and error is that the current method is capable of deriving the angular positions of the scatterers rather exactly using zero Doppler shifts; therefore, the

Table 3. Computational efficiency of the proposed method.

method	Root mean square error (m)	Computation Time (s)
Current method	0.0116	6.9
MUSIC [5]	0.0281	8.1
Conventional SAR	0.0664	5.2

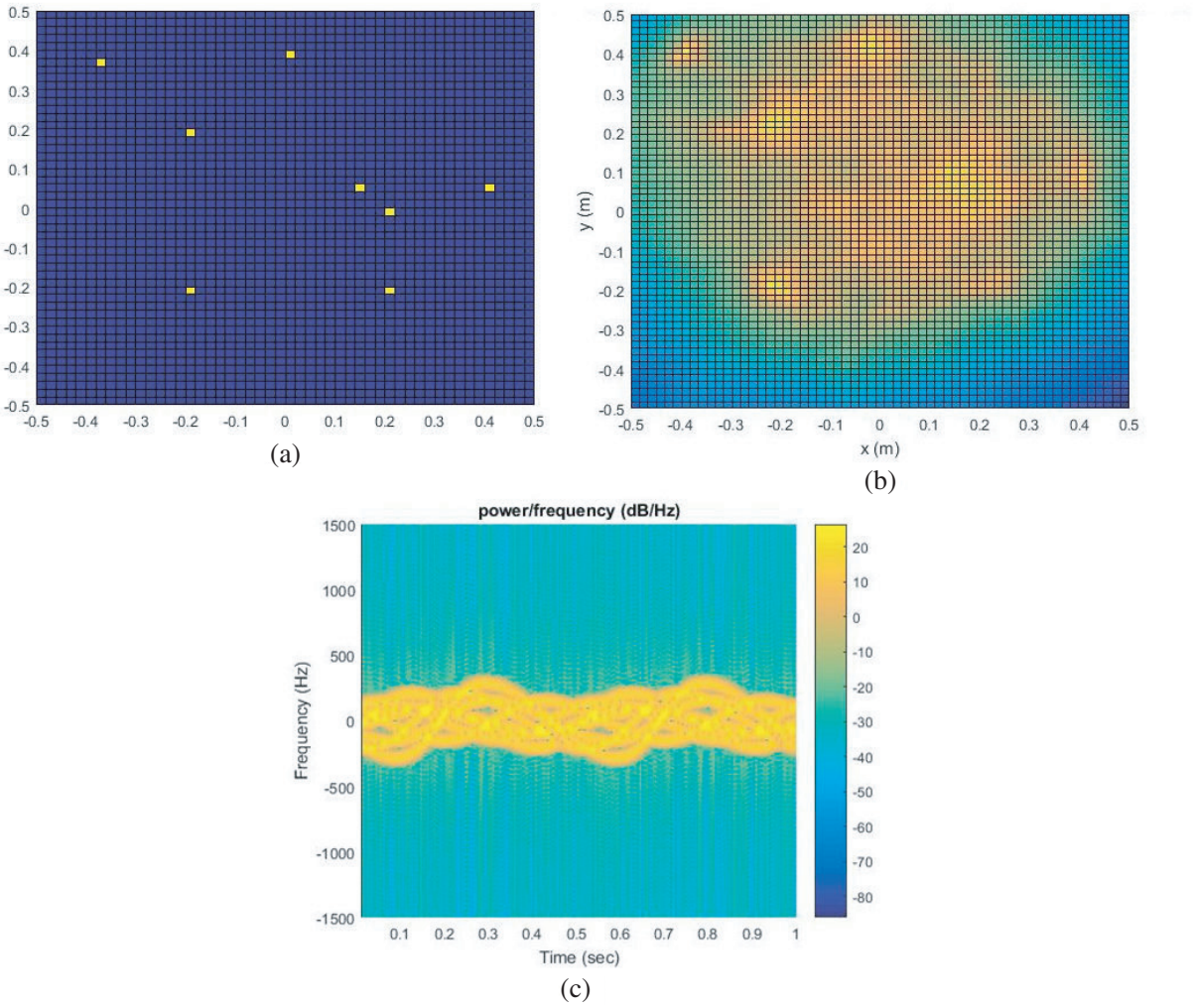

Figure 4. Random multi-point scatterer imaging. (a) Random multi-point scatterer. (b) Image. (c) Spectrum of the returned signal.

optimization does not operate on 2D function. Also it is worth mentioning that using nonsymmetric trajectories, this method will be capable of deriving the scatterers positions by locating the radar sampling points with zero Doppler shifts.

4. CONCLUSION

The aim of the study was to develop a novel and modest method for imaging the objects with strong scattering points based on Doppler phenomenon. The main advantages of the mentioned algorithm were novelty, simplicity, less computational time, and capability of operation as an additional method with the purpose of resolution improvement using unchanged setups. The method used radar movements and different Doppler shifts detected in the receiver in different sampling positions to obtain the scatterers' positions. Also, it is worth mentioning that the current method derives the angular position of objects by locating the radar sampling positions with zero Doppler shift before using optimization. The mentioned fact reduces the computational time of the method. This method is theoretically practicable using both coherent and non-coherent devices; however, according to the frequency resolution of the non-coherent devices, the results of the non-coherent devices would be more accurate. In the current paper, we study the imaging in 2D using circular geometry for radar path; however, this method is replicable for 3D imaging and other geometries, and it is possible to gain higher resolution using optimized

path. 3D imaging and optimization of radar path are recommended for further works. This method is applicable to different circumstances in the far field, so it is practical for remote sensing, navigation, and medical imaging in simple and high-contrast media, as mentioned earlier. Likewise, it can be used along with ultrasound technology in sonar and oceanography applications with higher resolution than the microwave.

REFERENCES

1. Browning, K. A. and R. Wexler, "The determination of kinematic properties of a wind field using Doppler radar," *Journal of Applied Meteorology*, Vol. 7, No. 1, 105–113, 1968.
2. Fornaro, G., D. Reale, and F. Serafino, "Four-dimensional SAR imaging for height estimation and monitoring of single and double scatterers," *IEEE Transactions on Geoscience and Remote Sensing*, Vol. 47, No. 1, 224–237, 2009.
3. Bertl, S., A. Dallinger, and J. Detlefsen, "Broadband circular interferometric millimetre-wave ISAR for threat detection," *Advances in Radio Science*, Vol. 5, No. 7, 147–151, 2007.
4. Lin, Y., W. Hong, W. Tan, et al., "Interferometric circular SAR method for three-dimensional imaging," *IEEE Geoscience and Remote Sensing Letters*, Vol. 8, No. 6, 1026–1030, 2011.
5. Solimene, R. and A. Dell'Aversano, "Some remarks on time-reversal MUSIC for two-dimensional thin PEC scatterers," *IEEE Geoscience and Remote Sensing Letters*, Vol. 11, No. 6, 1163–1167, 2014.
6. Chen, V. C., F. Li, S. S. Ho, et al., "Analysis of micro-Doppler signatures," *IEE Proceedings — Radar, Sonar and Navigation*, Vol. 150, No. 4, 271–276, 2012.
7. Zhang, Q., T. S. Yeo, H. S. Tan, et al., "Imaging of a moving target with rotating parts based on the Hough transform," *IEEE Transactions on Geoscience and Remote Sensing*, Vol. 46, No. 1, 291–299, 2008.
8. Wang, Y., "Inverse synthetic aperture radar imaging of manoeuvring target based on range-instantaneous-Doppler and range-instantaneous-chirp-rate algorithms," *IET Radar, Sonar and Navigation*, Vol. 6, No. 9, 921–928, 2012.
9. Stankovic, L., T. Thayaparan, M. Dakovic, et al., "Micro-Doppler removal in the radar imaging analysis," *IEEE Transactions on Aerospace and Electronic Systems*, Vol. 49, No. 2, 1234–1250, 2013.
10. Chen, V. C. and S. Qian, "Joint time-frequency transform for radar range-Doppler imaging," *IEEE Transactions on Aerospace and Electronic Systems*, Vol. 34, No. 2, 486–499, 1998.
11. Barbarossa, S. and A. Farina, "Detection and imaging of moving objects with synthetic aperture radar. Part 2: Joint time-frequency analysis by Wigner-Ville distribution," *IEE Proceedings F (Radar and Signal Processing)*, Vol. 139, No. 1, 89–97, 1992.
12. Moghimirad, E., A. Mahloojifar, and B. M. Asl, "Computational complexity reduction of synthetic aperture focus in ultrasound imaging using frequency-domain reconstruction," *Ultrasonic Imaging*, 2015.
13. Moses, R. L., L. C. Potter, and M. Cetin, "Wide-angle SAR imaging," *Defense and Security, International Society for Optics and Photonics*, 164–175, 2004.
14. Bjrck, A., *Numerical Methods for Least Squares Problems*, SIAM, 1996.
15. Homaifar, A., C. X. Qi, and S. H. Lai, "Constrained optimization via genetic algorithms," *Simulation*, Vol. 62, No. 4, 242–253, 1994.
16. Chen, V. C. and W. J. Miceli, "Time-varying spectral analysis for radar imaging of manoeuvring targets," *Radar, Sonar and Navigation, IEE Proceedings*, Vol. 145, No. 5, 262–268, 1998.
17. Fulop, S. A. and K. Fitz, "Algorithms for computing the time-corrected instantaneous frequency (reassigned) spectrogram, with applications," *J. Acoust. Soc. Am.*, Vol. 119, No. 1, 360–371, 2006.
18. Caorsi, S., M. Donelli, A. Lommi, and A. Massa, "Location and imaging of two-dimensional scatterers by using a particle swarm algorithm," *Journal of Electromagnetic Waves and Applications*, Vol. 18, No. 4, 481–494, 2004.

19. Donelli, M., I. J. Craddock, D. Gibbins, and M. Sarafianou, "A three-dimensional time domain microwave imaging method for breast cancer detection based on an evolutionary algorithm," *Progress In Electromagnetics Research M*, Vol. 18, 179–195, 2011.
20. Rocca, P., M. Donelli, G. L. Gragnani, and A. Massa, "Iterative multi-resolution retrieval of non-measurable equivalent currents for the imaging of dielectric objects," *Inverse Problems* Vol. 25, No. 5, 055004, 2009.
21. Franceschini, G., M. Donelli, R. Azaro, and A. Massa, "Inversion of phaseless total field data using a two-step strategy based on the iterative multiscaling approach," *IEEE Transactions on Geoscience and Remote Sensing*, Vol. 44, No. 12, 3527–3539, 2006.
22. Devaney, A. J., "Time reversal imaging of obscured targets from multistatic data," *IEEE Transactions on Antennas and Propagation*, Vol. 53, No. 5, 1600–1610, 2005.